Submit to: Inorganic Chemistry

Ultra-stable PtCo/Co_3O_4-SiO_2 Nanocomposite with Active Lattice Oxygen for Superior Catalytic Activity towards CO Oxidation

*Dandan Wu, [†a,b] Runping Jia,[†b] Ming Wen,[*a] Shuai Zhong,[a] Qingsheng Wu,[a] YongQing Fu [c] and Shuhong Yu [d]*

[a]School of Chemical Science and Engineering, Shanghai Key Laboratory of Chemical Assessment and Sustainability, Tongji University, 1239 Siping Road, Shanghai 200092, R. P. China.
[b]School of Materials Science and Engineering, Shanghai Institute of Technology, 100 Haiquan Road, Shanghai 201418, R. P. China.
[c]Faculty of Engineering and Environment, Northumbria University, Newcastle upon Tyne, NE1 8ST, UK.
[d]Department of Chemistry, University of Science and Technology of China, Hefei National Research Center for Physical Sciences at Microscale, 96 JinZhai Road, Hefei 230022, R. P. China.

KEYWORDS

PtCo/Co_3O_4-SiO_2, flower-like structure, CO oxidation, active lattice oxygen, long-term durability

ABSTRACT

Nanostructural catalyst with long-term durability under harsh conditions is very important for outstanding catalytic performance. Herein, a new ultra-stable PtCo/Co_3O_4-SiO_2 nanocatalyst was explored to improve the catalytic performance of carbon monoxide (CO) oxidation in virtue of the active surface lattice oxygen derived from strong metal-support interactions. Such structure can overcome the issues of the Co_3O_4-SiO_2 inactivation by water vapor and the Pt inferior activity at low temperature. Further, Co_3O_4-SiO_2 nanosheets endow superior structure stability under a high temperature up to 800 °C, which gives the long-term catalytic cyclability of PtCo/Co_3O_4-SiO_2

nanocomposites for CO oxidation. Moreover, the large specific surface areas (294 m^2/g) of the nanosheet structure can expose abundant active surface lattice oxygen, which significantly enhanced the catalytic activity of CO oxidation at 50 °C over 30 days, and without apparent aggregation of PtCo nanoparticles after 20 cycles from 50 °C to 400 °C. It can be expected to be a promising candidate for ultra-stable efficient catalyst.

1. INTRODUCTION

Many industrial catalytic processes, including carbon monoxide (CO) oxidation, CH_4 combustion, catalytic hydrogenation reaction, etc., are generally carried out over 300 °C, therefore, designing high-temperature-resistant catalysts with good performance become critically demanded.[1-5] Till now, nanocatalysts containing Pt have still received extensive attention for these applications.[6-9] However, Pt nanoparticles (NPs) are easily aggregated for minimizing their surface energy at a high temperature, which could result in serious activity dropping of catalysts. To solve this problem, some methods have been proposed.[10,11] For example, Pt NPs have been dispersed onto the support with large surface areas (e.g., CeO_2 or Al_2O_3), and thus can realize enhanced utilization of active-atoms thereby improving the catalytic activity. But the catalytic activity remains to be improved at temperatures <100 °C.[12-14] So it is yet an arduous challenge to construct Pt included nanocatalysts with a long cyclability within a much wider temperature range.

Owing to the special structure features, various two-dimensional (2D) nanomaterials have been investigated globally in recent years.[15,16] Hereinto, non-noble-metals nanosheets with an atomic-layer thickness, especially those with defective ones, have been proposed as a promising candidate to improve catalytic performance due to their abundant catalytic active sites.[17-21] It has been demonstrated that ultrathin CeO_2 nanosheets with surface pits

can exhibit an outstanding catalytic activity for CO oxidation.[22] However, it is difficult to maintain 2D nanostructure and activity at a high temperature because of high surface energy, which significantly restrict their practical catalysis applications. In order to stabilize the active components, silica (SiO_2) has been widely applied as a support or a shell in the heterogeneous catalysts, but this is still not good enough to restrain the aggregation of active components or to contact well with catalytic substrates.[23-25] To address the above issues, one way is to fabricate the 2D nanocomposite with the catalytic active components separated by SiO_2 nanosheets, which can not only increase the stability of active species, but also enlarge surface areas for the effective utilization of active atoms.

In this work, a unique heterostructure of PtCo/Co_3O_4-SiO_2 has been designed and successfully constructed through a galvanic replacement coprecipitation process followed by H_2 reduction, in which insitu alloying of PtCo anchored on Co_3O_4-SiO_2 nanosheets results in abundant active lattice oxygens. Such structure is expected to improve the catalytic activity of Pt at low temperature, meanwhile to overcome the catalysis limitation of Co_3O_4 under water vapour for CO oxidation. Thus, the obtained PtCo/Co_3O_4-SiO_2 catalysts can give rise to the following advantages for CO oxidation: i) Such nanoflower-like structure assembled by nanosheets leads to a mass of channels and large surface areas, which are beneficial for gas flow thereby immensely improving the catalyzation of CO oxidation; ii) The excellent thermal-stability of Co_3O_4-SiO_2 nanosheets can ensure the steady structure even at a high-temperature over 800 °C for long cycling catalytic activity; iii) The strong metal-support interactions (SMSI) between PtCo and Co_3O_4-SiO_2 can generate plentiful active lattices oxygens, which enable to significantly enhance catalytic performance at low temperature under water vapour. Therefore, the PtCo/Co_3O_4-SiO_2

structures exhibit an excellent stability at a high temperature, meanwhile, overcome the both issues of the Co_3O_4-SiO_2 inactivation by water vapor and the Pt inferior activity at low temperature. This work explores a new route in the development of ultra-stable hetero-nanocatalysts with 2D self-assembled structure for efficiently catalyzing CO oxidation at a wide temperature range in virtue of the active centers derived from SMSI.

2. EXPERIMENT SECTION

2.1. Chemicals

Copper chloride dihydrate ($CuCl_2 \cdot 2H_2O$, 99%), ethanol (C_2H_5OH, 99%), acetone (C_3H_6O, 99.5%) and chloroplatinic acid hexahydrate ($H_2PtCl_6 \cdot 6H_2O$ with Pt content ≥ 37%) were purchased from Sinopharm Chemical Reagent Co., Ltd., China. Cobalt chloride hexahydrate ($CoCl_2 \cdot 6H_2O$, 99.7%), sodium borohydride ($NaBH_4$, 98%), urea (CH_4N_2O, 99%) and hydrofluoric acid (HF, ≥ 40%) were purchased from Aladdin Reagents, Shanghai, China. All reagents were used without further purification. The silicon wafers were purchased from Zhejiang Lijing Silicon Material Co., Ltd. China., and cleaned with acetone, ethanol, and then the deionized water for three times before the usage.

2.2. Synthesis of Co_3O_4-SiO_2 nanoflower-spheres

The Co_3O_4-SiO_2 nanoflower-spheres catalyst was synthesized by a modified hydrothermal method. The typical synthesis process is described as follows: $CoCl_2 \cdot 6H_2O$ aqueous solution (15 mL, 5 mM) and $CuCl_2 \cdot 2H_2O$ aqueous solution (5 mL, 5 mM) were mixed in a Teflon-lined stainless steel autoclave. Then, a piece of 1cm×1cm silicon wafer and 200 mg of urea were added. After magnetic stirring for 10 min, the reaction system was sealed and heated at 140 ^oC in an oven for 8 hrs with a heating rate of 1 $^oC \cdot min^{-1}$. When the oven was cooled down to room temperature, the obtained products in the autoclave except for silicon wafer was collected by centrifugation,

and then alternately washed by ethanol and deionized water for three times and dried in a vacuum oven at 60 ^{o}C for 24 hrs. The Co_3O_4-SiO_2 catalyst was obtained by calcinating the dried powder in air at 600 ^{o}C for 5 hrs. In addition, 3D radial needle-like Co_3O_4 would be obtained, when only $CoCl_2 \cdot 6H_2O$ aqueous solution (15 mL, 5 mM) and urea (200 mg) were added to the Teflon-lined stainless steel autoclave.

2.3. Synthesis of PtCo/Co_3O_4-SiO_2 nanocomposite

In a typical preparation process, 50 mg of as-obtained Co_3O_4-SiO_2 nanocomposite was added to HF solution (10 mL, 0.04%) and stirred for 20 min; then the suspension was washed with deionized water. After that, H_2PtCl_6 solution (5 mL, 5 mM) was added to the washed suspension and subsequently ultrasonically dispersed for 2 hrs. The obtained solution was then placed in the freezer to ice-cold and rapidly injected a freshly prepared and ice-cold $NaBH_4$ aqueous solution (10 mL, 10 mM) under vigorous stirring. The resulting mixture was then left at room temperature for 5 hrs and the final precipitates of Pt/Co_3O_4-SiO_2 nanocomposites were collected by centrifugation and washed thoroughly. By further reducing Pt/Co_3O_4-SiO_2 nanocomposite in 5% H_2 at 400 ^{o}C for 1hr with a heating rate of 10 ^{o}C·min^{-1}, PtCo/Co_3O_4-SiO_2 nanocomposite catalyst can be obtained.

For comparison, the flower-like nanostructure of $PtCo_{sync}$/Co_3O_4-SiO_2 were also prepared by co-reduction alloy method, in which PtCo NPs were directly loaded on Co_3O_4-SiO_2 nanosheet. The specific synthetic steps were as follows: 50 mg Co_3O_4-SiO_2 nanocomposite was added to HF solution (10 mL, 0.04%) and stirred for 20 min; then the suspension was washed with deionized water. After that, $H_2PtCl_6 \cdot 6H_2O$ aqueous solution (5 mL, 5 mM) and $CoCl_2 \cdot 6H_2O$ aqueous solution (2 mL, 5 mM) were added to the washed suspension, and ultrasonically agitated for 2 hrs. The obtained solution was then placed in the freezer to ice-cold, and a freshly prepared, ice-cold

$NaBH_4$ aqueous solution (10 mL, 10 mM) was then rapidly injected under a vigorous stirring. The solutions was precipitated at room temperature for 5 hrs, and the precipitates were centrifuged, washed with deionized water and absolute ethanol repeatedly, and then dried in a vacuum oven at 60 ºC for 24 hrs to obtain $PtCo_{sync}/Co_3O_4$-SiO_2 nanocomposite catalyst.

2.4. Characterization

Field-emission scanning electron microscope (SEM, JEOL, S-4800) was used to investigate the morphology of the samples, and elemental compositions were analyzed by using an energy dispersive X-ray spectroscope (EDS), which was conducted at 20 keV on a TN5400 EDS instrument (Oxford). Microstructures of the materials were studied by using a high-resolution transmission electron microscope (HRTEM, JEOL JEM-2100EX, Japan). Powder X-ray diffraction (XRD) patterns were obtained by using a Bruker D8 (German) diffractometer with a Cu Kαradiation source (λ= 0.1541 nm) and a scanning angle (2θ) of 10°-90°, operated at 40 kV and 40 mA. The chemical states of elements were analyzed by using an X-ray photoelectron spectroscope (XPS, RBD-upgraded PHI-5000C ESCA system, Perkin Elmer) with Mg Kα radiation (hν=1486.6 eV). Before analyzing the XPS peaks, the binding energies of all the elements were calibrated using the containment carbon (C *1s*=284.6 eV) as the reference. The deconvolution of the XPS spectra was performed after subtracting the background of each peak using the Shirley. The Brunauer–Emmett–Teller (BET) surface areas were measured using the Micromeritics TRISTAR 3020. H_2 temperature-programmed reduction (H_2-TPR) was carried out on a Micromeritics AutoChem II 2920 automated catalyst characterization system. CO adsorption diffuse reflectance infrared Fourier-transform spectroscopy (CO DRIFTS) was performed on PerkinElmer Frontier FT-IR.

2.5. CO oxidation measurements

The activities of catalysts for CO oxidation were evaluated in a continuous flow fixed-bed quartz reactor under an atmospheric pressure. 50 mg catalysts were pressed, crushed, and sieved to the 40-60 mesh size range and diluted with 200 mg of quartz sand. The operation temperature was controlled using a thermocouple and adjusted in the range of 30 °C to 400 °C. Temperatures used in the catalytic tests were measured using a second thermocouple placed in the catalyst bed. Before each measurement, the catalysts were pre-treated with N_2 gas (50 ml·min^{-1}) at 300 °C for 1 hr, then a 2.0 vol.% CO/10 vol.% O_2/N_2 mixture (50 ml·min^{-1}) was introduced into the reactor, which corresponds to a gas hourly space velocity(GHSV) of 60,000 h^{-1}. The reactants and products were analyzed using on-line A90 gas chromatography (Shanghai Yimeng Electronic Technology Co., Ltd.). The column was a stainless steel tube with a diameter of 3 mm and was filled with a carbon molecular sieve chromatography packing. The detector used was a thermal conductivity detector (TCD). And the details of the equipment are shown in scheme S1. The catalytic oxidation activity of the catalyst is represented by the conversion rate of CO_2 generated by CO. The CO light-off temperature is 50% of CO conversion and represented by T_{50}; and the lowest complete conversion temperature of the CO is represented by T_{100}. The conversion rate (C) was calculated according to the following formula: $C=n(CO_{in})-n(CO_{out})\ /n(CO_{in})$

For a typical light-off run, the temperature was ramped with a rate of 2 °C·min^{-1} from 30 °C to 400 °C, and the data collection was performed after every 5 °C. Prior to data recording for each experiment, the temperature was stabilized for 5 min.

In a typical steady-state experiment, the system was adjusted to the measured temperature under N_2 flow at a heating rate of 10 °C·min^{-1}, and then replaced by the reaction mixture gas. The data were recorded every 12 hrs.

In a standard cycle experiment, the temperature was increased from 50 °C to 400 °C with a step of 25 °C. Before the measurement, the temperature was controlled to stabilize for 5 min. Once a cycle was finished, the reactor was cooled down to room temperature before new cycle was started.

3. RESULTS AND DISCUSSION

3.1. Mechanism of fabrication

The flower-like nanostructures of PtCo/Co_3O_4-SiO_2 have been successfully constructed, in which the structures were self-assembled by Co_3O_4-SiO_2 nanosheets with embedded PtCo nanoalloys (NAs) via the insitu reduction of H_2, as shown in Scheme 1. Firstly, $Co_3(Si_2O_5)_2(OH)_2$ nanoflower-spheres, the precursor of the Co_3O_4-SiO_2 nanocomposites, were fabricated by galvanic replacement coprecipitation process in a hydrothermal system. The reaction is initiated by the hydrolysis of urea, the subsequent product of NH_3 hydrolyzes to produce OH^- and react with Co^{2+} & SiO_3^{2-}. Then $Co_3(Si_2O_5)_2(OH)_2$ precursor were obtained, in which SiO_3^{2-} was derived from the replacement of Cu^{2+} with Si on the surface of silicon wafer, because $\phi Cu^{2+}/Cu$ (-0.222 V) is much higher than $\phi SiO_3^{2-}/Si$ (-1.697 V) in the alkaline solution. After the reaction, the surface of silicon wafer was then chemically deposited by a layer of copper, which can be confirmed by XRD analysis (Figure S1). As the surface of silicon wafer covered by a layer of Cu, $Co_3(Si_2O_5)_2(OH)_2$ complex was preferred to grow in the solution, rather than on the silicon wafer. In the hydrothermal reaction, the Cu^{2+} ions can not only control the generation rate of SiO_3^{2-}, but also react with NH_3 to form $[Cu(NH_3)_4]^{2+}$, therefore restrict the hydrolysis of NH_3 and then further control the co-precipitation rate of Co^{2+} and SiO_3^{2-} , which finally lead to the formation of 2D $Co_3(Si_2O_5)_2(OH)_2$ nanosheets precursor. In order to optimize the synthesis method and demonstrate the synthesis mechanism, we have selected different specifications

of silicon wafers and different additions of Cu^{2+} to react. The SEM was used to observe the morphologies of obtained samples, as shown in Figure S2 and S3. After the calcination, the precursors can be transformed into Co_3O_4-SiO_2 nanocomposites. Secondly, after treatment with HF, $PtCl_6^{2-}$ was absorbed on Co_3O_4-SiO_2 nanosheets then to be in-situ reduced and form Pt/Co_3O_4-SiO_2 composites. Finally, the further H_2 treatment gives rise to the heterostructured of PtCo/Co_3O_4-SiO_2, in which Pt induced the reduction of Co from the surrounding Co_3O_4 to form PtCo NAs, and results in the generation of active lattice oxygens as shown in Scheme 1B.[26,27]

Scheme 1. Schematic illustration of the fabrication process of PtCo/Co_3O_4-SiO_2 heterostructure.

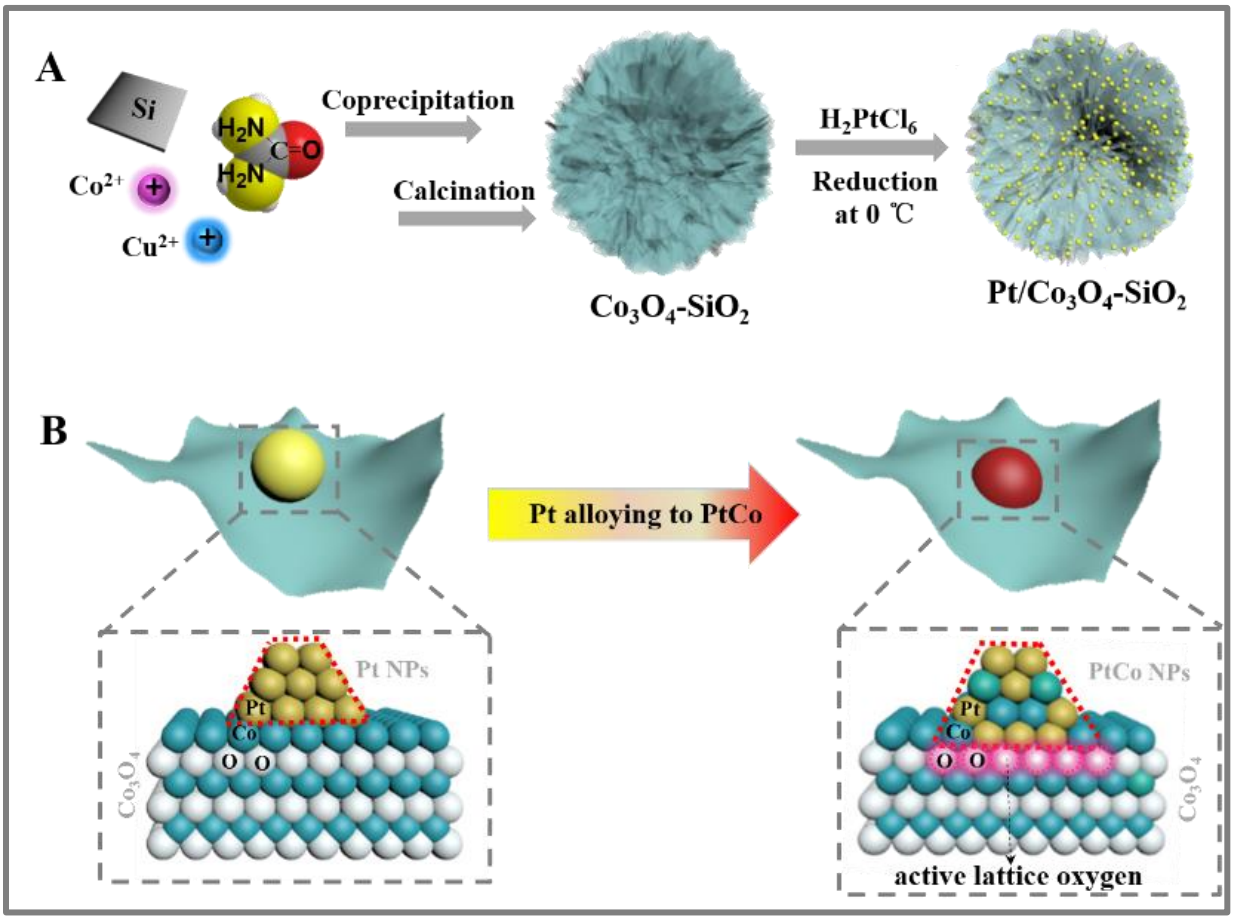

3.2. Morphologies and Structures

Morphologies and structures of PtCo/Co_3O_4-SiO_2 nanocomposites and contrast samples (Pt/Co_3O_4-SiO_2 and Co_3O_4-SiO_2) are characterized, shown in Figure 1. It can be clearly observed that Co_3O_4-SiO_2 support are nanoflower-spheres with an average diameter of 3.5 μm, self-assembled by numerous Co_3O_4-SiO_2 nanosheets (Figure 1A-E). Such structure is endowed with an extremely large surface area of 294 $m^2 \cdot g^{-1}$. The HRTEM image in Figure 1F presents a mixture of crystalline structures with a lattice spacing of 2.86 Å of Co_3O_4 (220) planes (marked with white box) and amorphous structures of SiO_2 (marked with black circle), further illustrates Co_3O_4 and SiO_2 embedded by each other. The inset SAED pattern shows polycrystalline diffraction rings, which can be indexed as the (220), (311), (400) and (422) facets of Co_3O_4, respectively. In Pt/Co_3O_4-SiO_2 nanocomposites, Figure 1G distinctly shows that the Pt NPs (~2 nm) are uniformly dispersed on the surface of Co_3O_4-SiO_2. Its HRTEM image reveals Pt (110) planes with a lattice spacing of 2.27 Å (marked in red box) besides Co_3O_4 (220) planes and amorphous SiO_2 (Figure 1H). The inset SAED pattern shows mixed diffraction ones of (111) and (220) facets from Pt and (311), (222) and (400) facets from Co_3O_4. The further H_2 treatment of the Pt/Co_3O_4-SiO_2 lead to the formation of PtCo/Co_3O_4-SiO_2 composites, in which the PtCo NPs with a mean diameter of 3 nm are uniformly anchored onto the Co_3O_4-SiO_2 nanosheets (Figure 1I). In addition, the mixed crystalline structure proved by the corresponding HRTEM image and SAED patterns confirms the formation of PtCo/Co_3O_4-SiO_2 nanocomposite (Figure 1J, K). Figure 1L shows EDS analysis results of the PtCo/Co_3O_4-SiO_2 (trace (a)) and Pt/Co_3O_4-SiO_2 (trace (b)) composites. Both of them contain Pt, Co, Si and O elements with the atomic ratio of Pt:Co:Si estimated to be 1:20:30, while Pt is absent in the Co_3O_4-SiO_2 nanocomposites (trace (c)). The element mappings are shown in Figure 1N-P, which can be overlapped with the corresponding SEM image (Figure 1M).

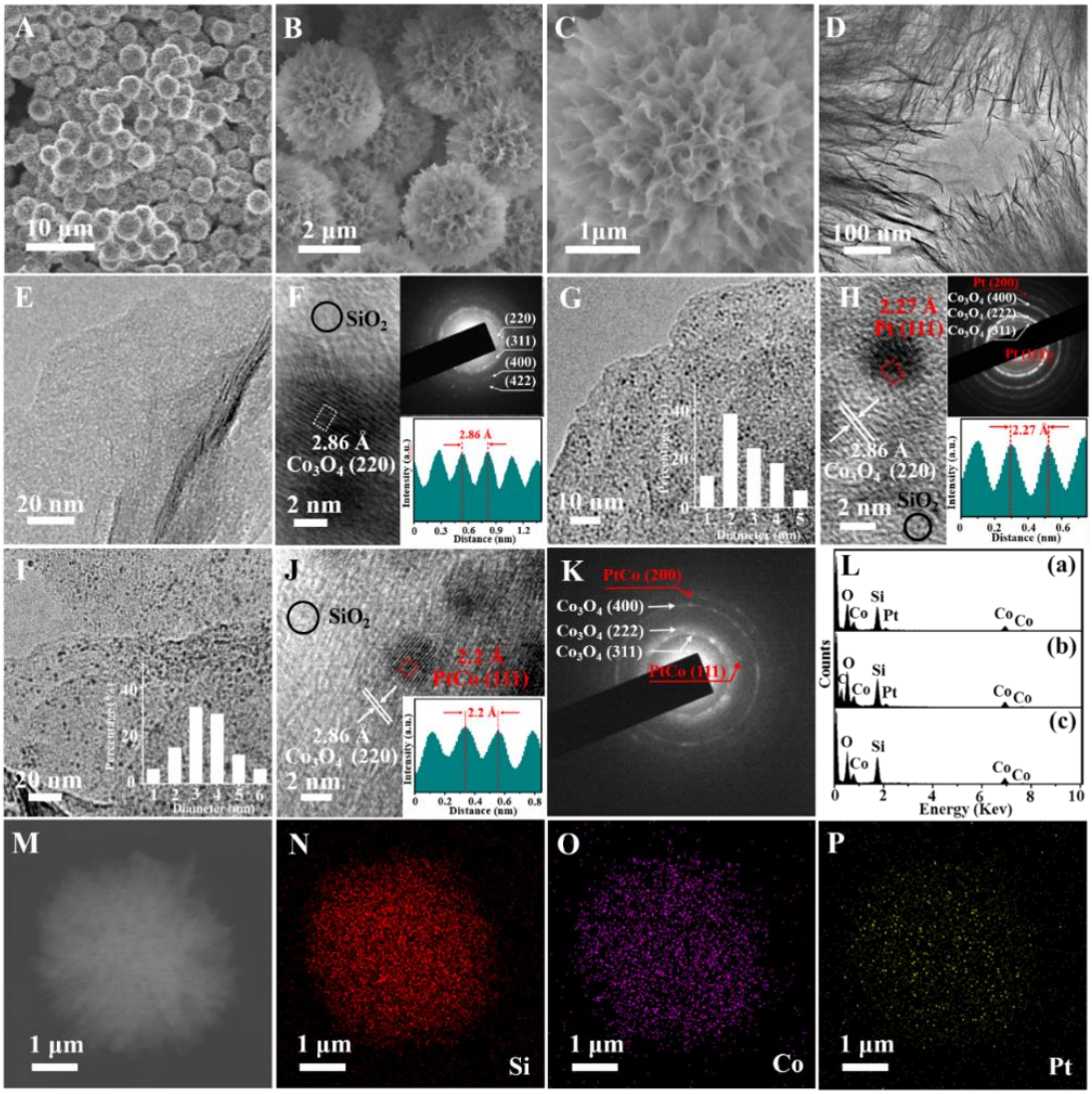

Figure 1. (A~C) SEM images and (D, E) TEM images with different magnification of Co_3O_4-SiO_2 nanocomposite; (F) HRTEM image of Co_3O_4-SiO_2 nanocomposite with inset SADE pattern; (G, H) TEM image with inset particle size distribution and HRTEM image with inset SADE pattern of Pt/Co_3O_4-SiO_2 nanocomposite; (I~K) TEM image with inset particle size distribution, HRTEM image and SADE pattern of PtCo/Co_3O_4-SiO_2 nanocomposite; (L) EDS analysis of PtCo/Co_3O_4-SiO_2 (a), Pt/Co_3O_4-SiO_2 (b) and Co_3O_4-SiO_2 (c) nanocomposites; (M~P) SEM image of PtCo/Co_3O_4-SiO_2 nanocomposite and elements mapping of Si, Co and Pt respectively.

Figure 2A shows the XRD patterns of the PtCo/Co_3O_4-SiO_2 nanocomposites and as-contrast samples. Because of the amorphous structure of SiO_2, only Co_3O_4 peaks can be observed in Co_3O_4-SiO_2 nanocomposite (curve (a)). The similar cases appear in Pt/Co_3O_4-SiO_2 (curve (b)) and

$PtCo/Co_3O_4$-SiO_2 (curve (c)), but without apparent peaks of Pt and PtCo alloys detected. This is mainly because these tiny NPs are uniformly distributed on the surface of Co_3O_4-SiO_2. [12,28] To further confirm the structure of these homodisperse NPs, Pt/Co_3O_4-SiO_2 and $PtCo/Co_3O_4$-SiO_2 samples were calcined at 873 K for 5 hrs in an argon environment. The XRD results of these samples were obtained and the results are shown in curves (d) and (e). In curve (d), we can clearly see three peaks at 39.7°, 46.2° and 67.4°, which can be indexed to the (111), (200) and (220) planes of Pt NPs (JCPDF No. 65-6828). Three peaks at 40.3°, 46.8° and 68.0° can be observed in curve (e), which are located between the standard peaks of Pt (JCPDF No. 65-6828) and Co (JCPDF No. 15-0806), indicating the existence of the PtCo NAs. [29,30]

To investigate the redox property of catalyst surface, H_2-TPR test has been conducted for the $PtCo/Co_3O_4$-SiO_2 nanocomposite and its contrast samples and shown in Figure 2B. There are two reduction peaks in both of the $PtCo_{sync}/Co_3O_4$-SiO_2 (curves b) and Pt/Co_3O_4-SiO_2 (curves c). The reduction peak in the low temperature range is linked with Co^{3+} reduction into Co^{2+}, during which the spinel structure of Co_3O_4 can be converted into CoO. The reduction peak in the high temperature range is related with the reduction of CoO to metallic Co.[31,32] Whereas, the H_2-TPR curve of the $PtCo/Co_3O_4$-SiO_2 composite (curves a) has three reduction peaks. The weak peak at 166 °C is attributed to the reduction of active lattice oxygen, which derived from SMSI via the in situ alloying of PtCo on Pt/Co_3O_4-SiO_2 nanosheets. [33] The active lattice oxygen can significantly enhance the activity of the CO catalytic reaction, especially at the low temperature.[13] In addition, the reduction peak of Co^{3+} reduced to Co^{2+} has been shifted to higher temperature, which is mainly due to the existence of SMSI between the PtCo NAs and Co_3O_4-SiO_2 support.[34]

To examine the role of the active lattice oxygen and PtCo alloy during reaction, we performed CO DRIFTS of $PtCo/Co_3O_4$-SiO_2 nanocomposite (Figure 2C) and compared the results with

Pt/Co_3O_4-SiO_2 nanocomposite (Figure 2D). The samples were placed in CO-filled infrared pool at 100°C, and spectral data were collected at 0min, 2min, 5min and 10min, respectively. A prominent symmetrical band at 2174 cm^{-1} and 2115 cm^{-1} can be observed in both samples, which are assigned to CO in the gas phase and linearly adsorbed CO on catalyst surface, respectively. In addition, a band at 2349 cm^{-1} was only seen on $PtCo/Co_3O_4$-SiO_2 for 2min, corresponding to CO_2, which can be considered as the reaction product of CO adsorbed on the catalyst surface with active lattice oxygen. After 5min, the band of CO_2 disappeared and the band of CO increased, indicating the product CO_2 can desorb in time without affecting CO reabsorption. Whereas for Pt/Co_3O_4-SiO_2, the band of CO keep increasing over time. Therefore, the active lattice oxygen and PtCo alloy plays an important role in the catalytic reaction of CO oxidation.

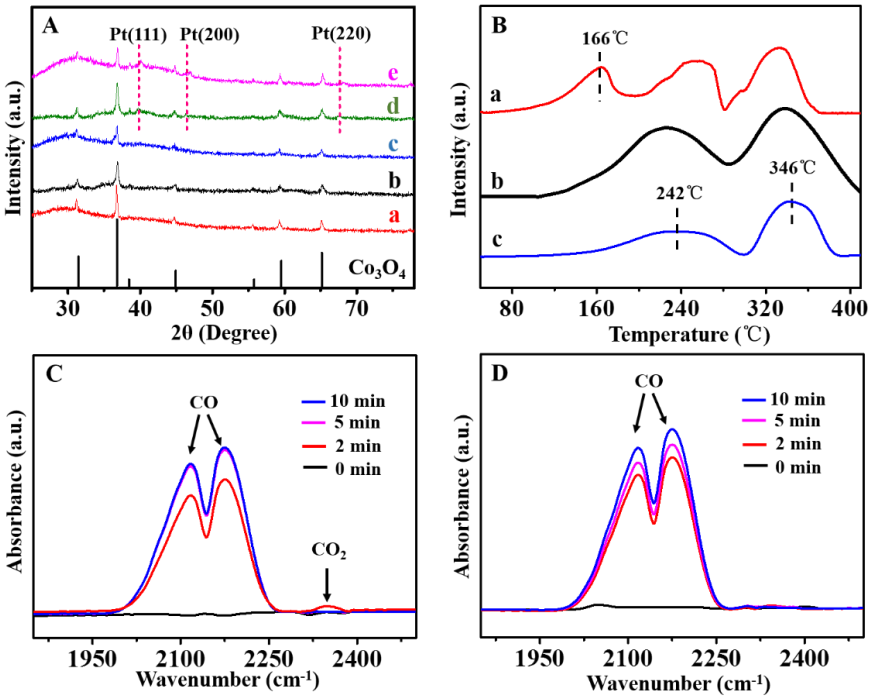

Figure 2. (A) XRD patterns of Co_3O_4-SiO_2 (a), Pt/Co_3O_4-SiO_2 (b), $PtCo/Co_3O_4$-SiO_2 (c), and the annealed Pt/Co_3O_4-SiO_2 (d), $PtCo/Co_3O_4$-SiO_2 (e) nanocomposites; (B) H_2-TPR profiles of $PtCo/Co_3O_4$-SiO_2 (a), $PtCo_{sync}/Co_3O_4$-SiO_2 (b) and Pt/Co_3O_4-SiO_2 (c) nanocomposites ; (C, D) CO DRIFTS of $PtCo/Co_3O_4$-SiO_2 (C) and Pt/Co_3O_4-SiO_2 (D).

XPS measurement was performed to further insight into the elemental valence information of Pt/Co_3O_4-SiO_2 and $PtCo/Co_3O_4$-SiO_2 nanocomposites. The survey spectra in Figure S4 clearly shows that both of the samples contain C, O, Si, Co, and Pt elements, which are consistent with the EDS results. In order to obtain the specific valence information of the elements, XPSPEAK41 peak software has been used to further analyze the characteristic peaks of Co 2p and Pt 4f. In Figure 3A, the peaks of Pt $4f_{7/2}$ and Pt $4f_{5/2}$ for Pt/Co_3O_4-SiO_2 can be deconvoluted into two pairs of peak, the peaks at 71.15 eV and 74.55 eV are attributed to Pt (0), the other peaks at 71.98 eV and 75.48 eV are related to Pt (II). Meanwhile, Pt $4f_{7/2}$ and Pt $4f_{5/2}$ of $PtCo/Co_3O_4$-SiO_2 in Figure 3B can be deconvoluted into two pairs of peak with binding energies of 71.19 eV & 74.7 eV and 72.02 eV & 75.54 eV, corresponding to Pt (0) and Pt (II), respectively. These peaks position of $PtCo/Co_3O_4$-SiO_2 shifts to the higher binding energy compared with those of Pt/Co_3O_4-SiO_2. This is mainly because that after the formation of PtCo alloy, the electron transfer between Pt and Co can shift the binding energy.[35,36] For the detailed XPS analysis of Co 2p spectra, Pt/Co_3O_4-SiO_2 (Figure 3C) and $PtCo/Co_3O_4$-SiO_2 (Figure 3D) have the same peak type, both of them are composed of main peaks and satellite peaks, but there is a difference in the position and FWHM of the peaks. Meanwhile, the analysis of XPSPEAK41 peak software shows that the main peaks of Co $2p_{3/2}$ and Co $2p_{1/2}$ for the Pt/Co_3O_4-SiO_2 in Figure 3C can be deconvoluted into two pairs of peak with binding energies of 779.8 eV & 795.6 eV and 782.2 eV & 797.2 eV, corresponding to Co (II) and Co (III), respectively. Whereas Figure 3D shows that the peaks of Co $2p_{3/2}$ and Co $2p_{1/2}$ for $PtCo/Co_3O_4$-SiO_2 can be deconvoluted into three pairs of peak with binding energies of 778.7 & 794.6, 780.0 & 795.8 and 782.1 eV & 797.3 eV, corresponding to Co (0), Co (II) and Co (III), respectively. The existence of Co (0) in $PtCo/Co_3O_4$-SiO_2 further demonstrates the successful

partial reduction of Co in Pt/Co_3O_4-SiO_2 nanocomposites. The peak located at the binding energy of 103.4 eV is related to the SiO_2 (Figure S5).

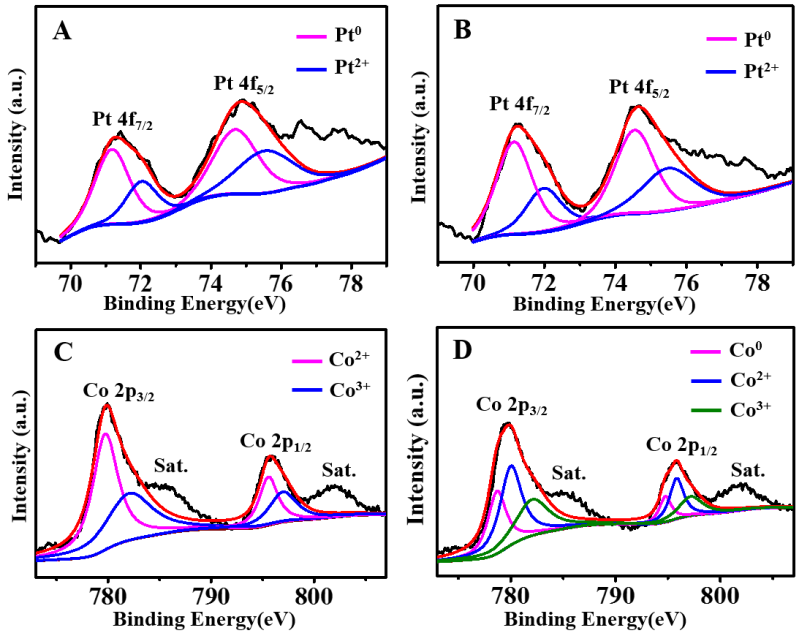

Figure 3. Detailed XPS analysis of Pt 4f spectra for Pt/Co_3O_4-SiO_2 (A) and PtCo/Co_3O_4-SiO_2 (B) as well as Co 2p spectra for Pt/Co_3O_4-SiO_2 (C) and PtCo/Co_3O_4-SiO_2 (D).

3.3. Catalytic Performance

Co_3O_4 has been widely used as the catalyst for efficient CO oxidation, however its performance stability is still limited by structure stability at high temperature and water vapour at low temperature.[37-39] In order to achieve high structure stability and large surface area for outstanding performance at high temperature, SiO_2 was embedded into Co_3O_4 to construct Co_3O_4-SiO_2 nanosheets. Meanwhile, as relevant density functional theory (DFT) calculation showed that water vapour can effectively promote CO oxidation performance of the Pt based catalyst,[40] Pt was introduced into catalyst system to overcome the negative effects of water vapour. In our case, the as-synthesized heterostructure of PtCo/Co_3O_4-SiO_2 is expected to address the issues of Co_3O_4 structure stability at high temperature and inactivation under water vapour, meanwhile, raising the

catalytic activity of Pt based catalyst at low temperature in virtue of active lattice oxygens derived from the insitu alloying of PtCo from Pt/Co_3O_4-SiO_2 under H_2.

In Figure 4A, for $PtCo/Co_3O_4$-SiO_2 nanocomposites, the CO light-off temperature (T_{50}) and the complete conversion temperature (T_{100}) are 50 °C and 115 °C, respectively, which are much lower than those of $PtCo_{sync}/Co_3O_4$-SiO_2 (T_{50} =105 °C and T_{100} =155 °C) and Pt/Co_3O_4-SiO_2 (T_{50} =115 °C and T_{100} =170 °C) . The reason can be suggested that the existence of abundant active lattice oxygens in the $PtCo/Co_3O_4$-SiO_2 nanocomposites can remarkably promote the catalytic reaction of CO oxidation. Therefore, the active lattice oxygen plays an important role in the catalytic reaction of CO oxidation. Meanwhile, the activity curve of Co_3O_4-SiO_2 nanocomposites shows a U shape, a lowest point of the CO conversion rate at 80 °C can be found, which is mainly due to the influence of water vapour.[41] In addition, the catalytic activity of CO oxidation for $PtCo/Co_3O_4$-SiO_2 nanocomposites have also been compared with other reported catalysts in the literature and summarized in the Table S1. Figure 4B shows the Arrhenius plots of the $PtCo/Co_3O_4$-SiO_2, $PtCo_{sync}/Co_3O_4$-SiO_2, Pt/Co_3O_4-SiO_2 and Co_3O_4-SiO_2 composites, according to the slope of the curves, their activation energies can be calculated to be 27.0 kJ/mol, 42.5 kJ/mol, 37.0 kJ/mol and 34.0 kJ/mol, respectively, further demonstrate the best catalytic activity of $PtCo/Co_3O_4$-SiO_2 nanocomposites. Since the light-off curves in Figure 4A can only indicates the short-term performance of the catalyst at a given temperature. In order to further investigate the catalytic activities of the synthesized catalysts in the low temperature and high temperature ranges, we have also tested the catalysts at a constant temperature (50 °C and 400 °C).

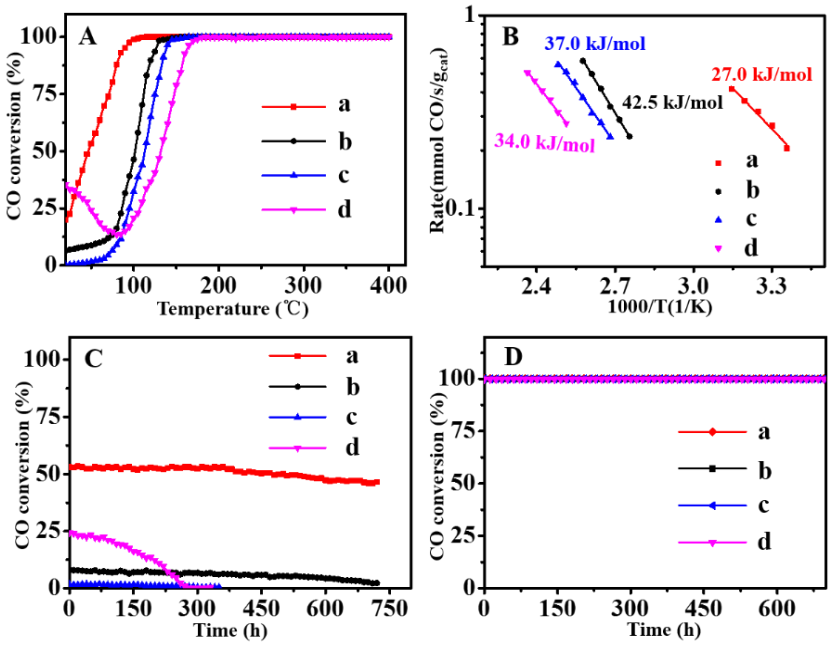

Figure 4. Temperature dependence of the activity (A) and Arrhenius plot for CO oxidation (B); Catalytic performance of CO oxidation at a constant temperature of 50 °C (C) and 400 °C (D) for PtCo/Co_3O_4-SiO_2 (a), $PtCo_{sync}$/Co_3O_4-SiO_2 (b), Pt/Co_3O_4-SiO_2 (c) and Co_3O_4-SiO_2 (d).

Figure 4C shows the CO conversion rate of PtCo/Co_3O_4-SiO_2 nanocomposites and other contrast catalysts, which have been continuously catalysed at 50 °C for 30 days. It can be clearly seen that the Pt/Co_3O_4-SiO_2 nanocomposites have little catalytic activity, and the activity of $PtCo_{sync}$/Co_3O_4-SiO_2 is much lower than that of the PtCo/Co_3O_4-SiO_2, indicating the formation of PtCo NAs and the active surface lattice oxygens can effectively enhance the catalytic oxidation activity in a low temperature environment. In addition, we can clearly see that catalytic activity of PtCo/Co_3O_4-SiO_2 nanocomposites has no significant decrease after 30 days catalysis reaction, by contrast, the catalytic activity of Co_3O_4-SiO_2 nanocomposites is decreased sharply after 100 hrs, which mainly because the catalyst surface was deactivated by the water vapour adsorption. Meanwhile, under the high temperature reaction environment of 400 °C, the CO conversion rates for all the synthesized catalysts are 100%, even after 30 days (Figure 4D). It illustrates that the

Co_3O_4-SiO_2 support plays a vital role in the catalysis under a high temperature environment. The excellent thermal stability of as-prepared Co_3O_4-SiO_2 nanocomposite can be demonstrated by heat treatment at 800 °C in air for 10 hrs (Figure S6).

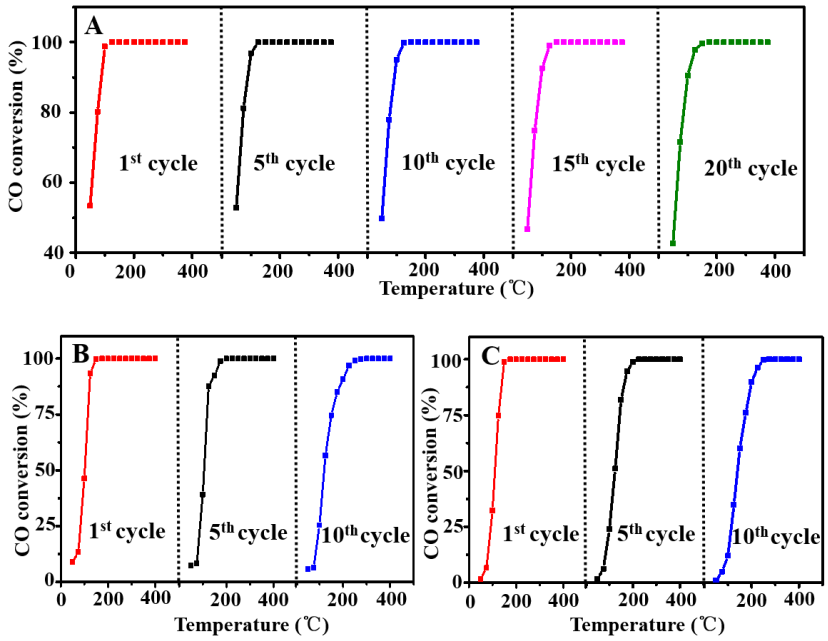

Figure 5. Conversion rate of CO from 50 to 400 °C with 20 cycles and 10 cycles for PtCo/Co_3O_4-SiO_2 (A), $PtCo_{sync}$/Co_3O_4-SiO_2 (B) and Pt/Co_3O_4-SiO_2 (C)

For further understand the high temperature thermal cycle stability of the synthesized catalysts, we conducted the cyclic catalytic tests from 50 °C to 400 °C. Figure 5A shows the CO conversion rates of PtCo/Co_3O_4-SiO_2 composite cycled for 20 times. The complete conversion temperature T_{100} has little increase after 20 cycles. Whereas for the $PtCo_{sync}$/Co_3O_4-SiO_2 (Figure 5B) and Pt/Co_3O_4-SiO_2 (Figure 5C) nanocomposites after 10 cycles catalysis, the T_{100} values are increased from 155 °C to 300 °C and 170 °C to 275 °C, respectively. The morphology and structure of the reacted catalyst have been further investigated by TEM (Figure S7) and XRD characterization (Figure S8). Severe agglomeration can be observed for the $PtCo_{sync}$/Co_3O_4-SiO_2 and Pt/Co_3O_4-SiO_2 nanocomposites, whereas the PtCo/Co_3O_4-SiO_2 only has little increase of the particle size

and there is no obvious change in the phase except adding a broad peak of PtCo alloy, which is mainly due to the increase in the particle size. This demonstrates that the heterostructure of the PtCo/Co_3O_4-SiO_2 has better structural stability relative to other nanocomposites, and thus has better cycling stability, which is mainly due to the existence of SMSI between the embedded PtCo NAs and Co_3O_4-SiO_2 support.

Scheme 2. Illustration of the catalysis mechanism of the CO oxidation reaction over PtCo/Co_3O_4-SiO_2 nanocomposites.

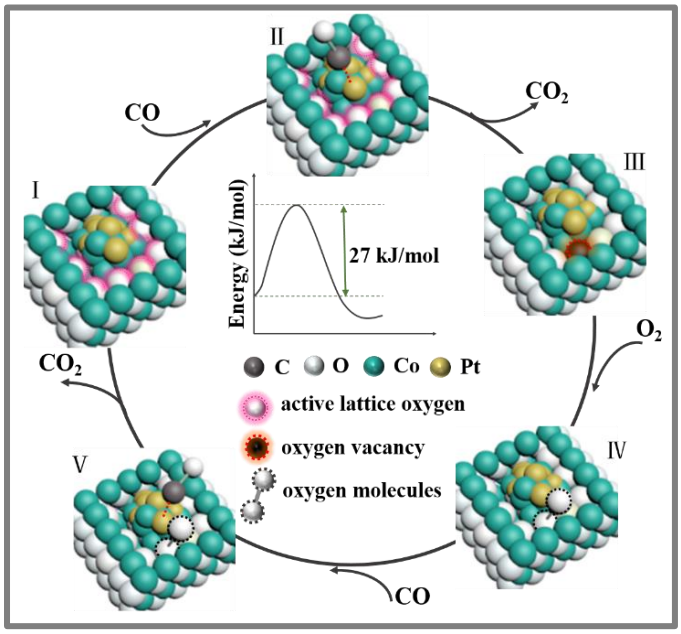

Based on the results of structural characterizations and performance measurements, the catalysis mechanism of the PtCo/Co_3O_4-SiO_2 nanocomposite has been proposed, as illustrated in Scheme 2. The CO catalytic oxidation can be assumed as a typical gas-solid heterogeneous catalytic reaction, thus the surface microelectronic structures and the specific surface areas of the catalyst have significant influences on its performance. CO oxidation over metallic Pt supported on reducible oxides follows a Mars-van Krevelen reaction mechanism. According to this mechanism, the active lattice oxygens, generated by the insitu alloying of PtCo on Co_3O_4-SiO_2 under H_2 reduction treatment, is responsible for the catalytic reaction. Therefore, over the catalyst of

$PtCo/Co_3O_4$-SiO_2 composites, CO is preferentially adsorbed onto the PtCo alloy and then reacts with the active lattice oxygen in its vicinity. [33,42,43] Then the O_2 molecules will fill the oxygen vacancies caused by the reacted lattice oxygen, thus the adsorbed O_2 molecules can be activated and dissociated to easily react with the CO. In addition, the PtCo NAs can weaken the strong absorption of the product CO_2 with Pt which would prevent the re-adsorption of CO at the active sites, thus $PtCo/Co_3O_4$-SiO_2 nanocatalyst have higher catalytic activity and cycle stability than Pt/Co_3O_4-SiO_2 nanocatalyst. When the reaction occurs at a high temperature, the influence of the active surface lattice oxygen on the catalytic performance can be significantly decreased, because the high temperature environment is favorable for the breaking of chemical bonds. Therefore, there are no apparent differences in the catalytic activities of CO oxidation among $PtCo/Co_3O_4$-SiO_2, $PtCo_{sync}/Co_3O_4$-SiO_2, and Pt/Co_3O_4-SiO_2 at high temperatures.

4. Conclusion

In summary, we have designed a flower-like structure of $PtCo/Co_3O_4$-SiO_2 composite, which has been obtained through a galvanic replacement coprecipitation process with subsequent H_2 reduction. The large specific surface areas and excellent structure stability of Co_3O_4-SiO_2 significantly enhance the catalytic activity and thermal cycling stability for catalyzing CO oxidation, meanwhile, the abundant active lattice oxygens and the SMSI between PtCo NAs and Co_3O_4-SiO_2 support remarkably improve the inferior activity of Pt based catalyst at low temperature. Hence, the $PtCo/Co_3O_4$-SiO_2 nanocomposites present an outstanding enhanced catalytic activity at low temperature and long-term catalytic cyclability for CO oxidation. This work opens up a new way to design a thermostable nanostructures by embedding SiO_2 nanosheets and improve the catalytic activity of catalysts by introducing active centers.

ASSOCIATED CONTENT

Supporting Information

SEM and TEM images, XRD and XPS patterns. This material is available free of charge via the Internet at http://pubs.acs.org.

AUTHOR INFORMATION

Corresponding Author

* E-mail: m_wen@tongji.edu.cn; Fax: (+86) -21-65981097

ORCID

Ming Wen: 0000-0002-2327-5459

Qingsheng Wu: 0000-0002-2371-5805

Author Contributions

†These authors contributed equally to this work.

Notes

The authors declare no competing financial interest.

ACKNOWLEDGMENT

This work was financially supported by the National Natural Science Foundation of China (NSFC Nos: 21771140, 51271132 and 91222103). UK Engineering and Physical Sciences Research (EPSRC, EP/P018998), Newton Mobility Grant (IE161019) through Royal Society UK and NSFC.

ABBREVIATIONS

NPs, nanoparticles; 2D, two-dimensional; SMSI, strong metal-support interactions; XRD, Powder X-ray diffraction; SEM, scanning electron microscopy; TEM, transmission electron microscopy; HRTEM, high resolution TEM; SAED, selected area electron diffraction; EDS, energy dispersive X-ray spectroscopy; XPS, X-ray photoelectron spectroscopy; BET, Brunauer–Emmett–Teller; H_2-TPR, H_2 temperature-programmed reduction; CO DRIFTS, CO adsorption diffuse reflectance infrared Fourier-transform spectroscopy; T_{50}, light-off temperature; T_{100}, complete conversion temperature; NAs, nanoalloys.

REFERENCES

[1] Li, Z.; Li, M.; Bian, Z.; Kathiraser, Y.; Kawi, S. Design of Highly Stable and Selective Core/Yolk-Shell Nanocatalysts-A Review. *Appl. Catal. B* **2016**, *188*, 324-341.

[2] Xiong, H.; Lin, S.; Goetze, J.; Pletcher, P.; Guo, H.; Kovarik, L.; Artyushkova, K.; Weckhuysen, BM.; Datye, AK. Thermally Stable and Regenerable Pt-Sn Clusters for Propane Dehydrogenation Prepared via Atom Trapping on Ceria. *Angew. Chem. Int. Ed*. **2017**, *56*, 8986-8991.

[3] Souza, M. M. V. M.; Schmal, M. Methane Conversion to Synthesis Gas by Partial Oxidation and CO_2 Reforming over Supported Platinum Catalysts. *Catal. Lett*. **2003**, *91*, 11-17.

[4] Guo, Z.; Liu, B.; Zhang, Q. H.; Deng, W. P.; Wang, Y.; Yang, Y. H.; Recent Advances in Heterogeneous Slective Oxidation Catalysis for Sustainable Chemistry, *Chem. Soc. Rev.* **2014**, 43, 3480-3524.

[5] Arai, H.; Machida, M. Thermal Stabilization of Catalyst Supports and Their Application to High-temperature Catalytic Combustion. *Appl. Catal. A* **1996**, *138*, 161-176.

[6] Chen, A.; Holt-Hindle, P.; Platinum-Based Nanostructured Materials: Synthesis, Properties, and Applications. *Chem. Rev*. **2010**, *110*, 3767-3804.

[7] Allian, A. D.; Takanabe, K.; Fujdala, K. L.; Hao, X.; Iglesia, E. Chemisorption of CO and Mechanism of CO Oxidation on Supported Platinum Nanoclusters. *J. Am. Chem. Soc*. **2011**, *133*, 4498-4517.

[8] Chen, W. L.; Ma, Y. L.; Li, F.; Pan, L.; Gao, W. P.; Xiang, Q.; Shang, W.; Song, C. Y.; Tao, P.; Zhu, H.; Pan, X. Q.; Deng, T.; Wu, J. B. Strong Electronic Interaction of Amorphous Fe_2O_3 Nanosheets with Single-Atom Pt toward Enhanced Carbon Monoxide Oxidation. *Adv. Funct. Mater.* **2019**, 1904278.

[9] Bonanni, S.; Aït-Mansour, K.; Harbich, W.; Brune, H. Effect of The TiO_2 Reduction State on The Catalytic CO Oxidation on Deposited Size-selected Pt Clusters. *J. Am. Chem. Soc*. **2012**, *134*, 3445-3450.

[10] Wu, K.; Zhou, L.; Jia, C. J.; Sun, L.; Yan, C. H. Pt-embedded-CeO_2 Hollow Spheres for Enhancing CO Oxidation Performance. *Mater. Chem. Front.* **2017**, *1*, 1754-1763.

[11] Zhou, H. P.; Wu, H. S.; Shen, J.; Yin, A. X.; Sun, L. D.; Yan, C. H. Thermally Stable Pt/CeO_2 Hetero-nanocomposites With High Catalytic Activity. *J. Am. Chem. Soc*. **2010**, *132*, 4998-4999.

[12] Jones, J.; Xiong, H.; Delariva, A. T.; Peterson, E. J.; Pham, H.; Challa, S. R.; Qi, G.; Oh, S.; Wiebenga, M. H.; Hernández, X. I. P.; Wang, Y.; Datye, A. K. Thermally Stable Single-atom Platinum-on-ceria Catalysts via Atom Trapping. *Science* **2016**, *353*, 150–154.

[13] Qiao, B.T.; Wang, A. Q.; Yang, X.F.; Allard, L. F.; Jiang, Z.; Cui, Y. T.; Liu, J. Y.; Li, J.; Zhang, T. Single-atom Catalysis of CO Oxidation Using Pt/FeO_x. *Nat. Chem*. **2011**, *3*, 634–641.

[14] Zhang, Z. L.; Zhu, Y. H.; Asakura, H.; Zhang, B.; Zhang, J. G.; Zhou, M. X.; Han, Y.; Tanaka, T.; Wang, A. Q.; Zhang, T.; Yan, N. Thermally Stable Single Atom Pt/m-Al_2O_3 for Selective Hydrogenation and CO Oxidation. *Nat. Commun*. **2017**, *8*, ncomms16100.

[15] Tan, C. L.; Cao, X. H.; Wu, X. J.; He, Q. Y.; Yang, J.; Zhang, X.; Chen, J. Z.; Zhao, W.; Han, S. K.; Nam, G. H.; Sindoro, M.; Zhang, H. Recent Advances in Ultrathin Two-dimensional Nanomaterials. *Chem. Rev*. **2017**, *117(9)*, 6225-6331.

[16] Zhang, H. Ultrathin Two-dimensional Nanomaterials. *ACS nano* **2015**, *9*, 9451-9469.

[17] Zhang, X.; Xie, Y. Recent Advances in Free-standing Two-dimensional Crystals with Atomic Thickness：Design, Assembly and Transfer Strategies. *Chem. Soc. Rev*. **2013**, *42*, 8187-8199.

[18] Sun, Y.; Gao, S.; Xie, Y. Atomically-thick Two-dimensional Crystals: Electronic Structure Regulation and Energy Device Construction. *Chem. Soc. Rev*. **2014**, *43*, 530-546.

[19] Wu, D. D.; Wen, M.; Lin, X. J.; Wu, Q. S.; Gu, C.; Chen, H. X. A NiCo/NiO-CoO_x Ultrathin Layered Catalyst with Strong Basic Sites for High-performance H_2 Generation from Hydrous Hydrazine. *J. Mater. Chem. A* **2016**, *4*, 6595-6602.

[20] Wu, D. D.; Wen, M.; Gu, C.; Wu, Q. S. 2D NiFe/CeO_2 Basic-site-enhanced Catalyst via In-situ Topotactic Reduction for Selectively Catalyzing the H_2 Generation from $N_2H_4 \cdot H_2O$. *ACS Appl. Mater. Interfaces* **2017**, *9*, 16103-16108.

[21] Gu, C.; Wu, D. D.; Wen, M.; Wu, Q. S. A Freestanding SiO_2 Ultrathin Membrane with NiCu Nanoparticles Embedded on Its Double Surfaces for Catalyzing Nitro-amination. *Dalton Trans*. **2018**, *47*, 7083-7089.

[22] Sun, Y.; Liu, Q.; Gao, S.; Cheng, H.; Xie, Y. Pits Confined in Ultrathin Cerium (IV) Oxide for Studying Catalytic Centers in Carbon Monoxide Oxidation. *Nat. Commun*. **2013**, *4*, 2899.

[23] Hu, Y.; Tao, K.; Wu, C.; Zhou, C.; Yin, H.; Zhou, S. Size-controlled Synthesis of Highly Stable and Active Pd@SiO_2 Core-shell Nanocatalysts for Hydrogenation of Nitrobenzene. *J. Phys. Chem. C* **2013**, *138*, 8974–8982.

[24] Masoud, N.; Delannoy, L; Schaink, H.; Eerden, A. V. D.; Rijk, J. W. D.; Silva, T. A. G.; Banerjee, D.; Meeldijk, J. D.; Jong, K. P. D.; Louis, C.; Jongh, P. E. D. Superior Stability of Au/SiO_2 Compared to Au/TiO_2 Catalysts for the Selective Hydrogenation of Butadiene . *ACS Catal*. **2017**, *7*, 5594-5603.

[25] Zhu, S.; Lian, X.; Fan, T.; Chen, Z.; Dong, Y.; Weng, W.; Yi, X.; Fang, W. Thermally Stable Core-shell Ni/nanorod-CeO_2@SiO_2 Catalyst for Partial Oxidation of Methane at High Temperatures. *Nanoscale* **2018**, *10*, 14031-14038.

[26] Fang, H.; Yang, J. H.; Wen, M.; Wu, Q. S. Nanoalloy Materials for Chemical Catalysis. *Adv. Mater*. **2018**, 1705698.

[27] Wang, D.; Li, Y. One-pot Protocol for Au-based Hybrid Magnetic Nanostructures via a Noble-metal-induced Reduction Process. *J. Am. Chem. Soc*. **2010**, *132*, 6280-6281.

[28] Zhang, R. B.; Lu, K.; Zong, L. J.; Tong, S.; Wang, X. W.; Feng, G. Gold Supported on Ceria Nanotubes for CO Oxidation. *Appl. Surf. Sci.* **2017**, *416*, 183-190.

[29] Wang, H. L.; Yan, J. M.; Wang, Z. L.; O, S.; Jiang, Q. Highly Efficient Hydrogen Generation from Hydrous Hydrazine over Amorphous $Ni_{0.9}Pt_{0.1}/Ce_2O_3$ Nanocatalyst at Room Temperature. *J. Mater. Chem. A* **2013**, *1*, 14957-14962.

[30] Wu, D. D.; Zhang, Y. Q.; Wen, M.; Fang, H.; Wu, Q. S. Fe_3O_4/FeNi Embedded Nanostructure and Its Kinetic Law for Selective Catalytic Reduction of *p*-nitrophenyl Compounds. *Inorg. Chem*. **2017**, *56*, 5152-5157.

[31] Tang, C. W.; Kuo, M. C.; Lin, C. J.; Wang, C. B.; Chien, S. H. Evaluation of Carbon Monoxide Oxidation Over CeO_2/Co_3O_4 Catalysts：Effect of Ceria Loading. *Catal. Today* **2008**, *131*, 520-525.

[32] Min, K.; Min, W. S.; Chang, H. L. Catalytic Carbon Monoxide Oxidation over CoO_x /CeO_2 Composite Catalysts. *Appl. Catal. A* **2003**, *251*, 143-156.

[33] Nie, L.; Mei, D.; Xiong, H.; Peng, B.; Ren, Z.; Hernandez,X.I.P.; DeLaRiva, A.; Wang, M.; Engelhard, M.H.; Kovarik, L.; Datye, A.K.; Wang, Y. Activation of Surface Lattice Oxygen in Single-atom Pt/CeO_2 for Low-temperature CO Oxidation. *Science* **2017**, *358*, 1419-1423.

[34] Tang, C. W.; Kuo, C. C.; Kuo, M. C.; Wang, C. B.; Chien, S. H. Influence of Pretreatment Conditions on Low-temperature Carbon Monoxide Oxidation over CeO_2/Co_3O_4 Catalysts. *Appl. Catal. A* **2006**, *309*, 37-43.

[35] Fang, H.; Chen, Y.; Wen, M.; Wu, Q. S.; Zhu, Q. J. SnNi Nanoneedles Assembled 3D Radial Nanostructure Loaded with SnNiPt Nanoparticles： Towards Enhanced Electrocatalysis Performance for Methanol Oxidation. *Nano Res*. **2017**, *10*, 3929-.

[36] Wang, W.; Wang, Z. Y.; Wang, J. J.; Zhong, C. J.; Liu, C. J. Highly Active and Stable Pt–Pd Alloy Catalysts Synthesized by Room-Temperature Electron Reduction for Oxygen Reduction Reaction. *Adv. Sci.* **2017**, *4*, 1600486.

[37] Xie, X.; Li, Y.; Liu, Z. Q.; Haruta, M.; Shen, W. Low-Temperature Oxidation of CO Catalysed By Co_3O_4 Nanorods. *Nature* **2009**, *458*, 746-749.

[38] Tüysüz, H.; Comotti M.; Schüth, F. Ordered Mesoporous Co_3O_4 as Highly Active Catalyst for Low Temperature CO-oxidation. *Chem. Commun*. **2008**, *34*, 4022-4024.

[39] Liotta, L. F.; Wu, H.; Pantaleo, G.; Venezia, A. M. Co_3O_4 Nanocrystals and Co_3O_4-MO_x Binary Oxides for CO, CH_4 and VOC Oxidation at Low Temperatures: A Review. *Catal. Sci. Technol*. **2013**, *3*, 3085-3102.

[40] Wang, H.; Richard, K.; Guo, Y.; Lu, G.Z.; Hu, P. Structural Origin： Water Deactivates Metal Oxides to CO Oxidation And Promotes Low-temperature CO Oxidation With Metals. *Angew. Chem., Int. Ed*, **2012**, *51(27)*, 6657-6661.

[41] Jia, C. J.; Schwickardi, M.; Weidenthaler, C.; Schmidt, W.; Korhonen, S.; Weckhuysen, B. M.; Schüth, F. Co_3O_4-SiO_2 Nanocomposite： A Very Active Catalyst for CO Oxidation with Unusual Catalytic Behavior. *J. Am. Chem. Soc.* **2011**, *133*, 11279-11288.

[42] Kopelent, R.; van Bokhoven, J.A.; Szlachetko, J.; Edebeli, J.; Paun, C.; Nachtegaal, M.; Safonova, O.V. Catalytically Active and Spectator Ce^{3+} In Ceria-Supported Metal Catalysts. *Angew. Chem., Int. Ed.* **2015**, *54*, 8728-8731.

[43] Liu, H. H.; Wang, Y.; Jia, A. P.; Wang, S. Y.; Luo, M. F.; Lu, J. Q. Oxygen Vacancy Promoted CO Oxidation over Pt/CeO_2 Catalysts: A Reaction at $Pt\text{-}CeO_2$ Interface. *Applied Surface Science* **2014**, *314*, 725-734.

Table of Contents

An ultra-stable $PtCo/Co_3O_4\text{-}SiO_2$ nanocatalyst with active surface lattice oxygen have been explored to overcome the issues of $Co_3O_4\text{-}SiO_2$ inactivation by water vapor and the Pt inferior activity at low temperature for catalyzing CO oxidation.

Keywords: $PtCo/Co_3O_4\text{-}SiO_2$, flower-like structure, CO oxidation, active lattice oxygen, long-term durability

Authors:

Dandan Wu,[†a,b,] Runping Jia[†,b,] Ming Wen[*,a,] Shuai Zhong[a], Qingsheng Wu[a], YongQing Fu[c], Shuhong Yu[d],

Title:

Ultra-stable $PtCo/Co_3O_4\text{-}SiO_2$ Nanocomposite with Active Lattice Oxygen for Superior Catalytic Activity towards CO Oxidation